Toxicology 299 (2012) 112–124

Contents lists available at SciVerse ScienceDirect

Toxicology

journal homepage: www.elsevier.com/locate/toxicol

Implication of oxidative stress in size-dependent toxicity of silica nanoparticles in kidney cells

Isabelle Passagne[a,*], Marie Morille[b], Marine Rousset[a], Igor Pujalté[a], Béatrice L'Azou[a]

[a] University Bordeaux, Pharmacochimie, FRE3396, F-33000 Bordeaux, France
[b] LUNAM Université, Ingénierie de la Vectorisation Particulaire, INSERM U646, F-49933 Angers, France

ARTICLE INFO

Article history:
Received 30 March 2012
Received in revised form 9 May 2012
Accepted 14 May 2012
Available online 22 May 2012

Keywords:
Silica
SiO_2
Nanoparticles
Cytotoxicity
Oxidative stress
Kidney

ABSTRACT

Silica nanoparticles (nano-SiO_2) are one of the most popular nanomaterials used in industrial manufacturing, synthesis, engineering and medicine. While inhalation of nanoparticles causes pulmonary damage, nano-SiO_2 can be transported into the blood and deposit in target organs where they exert potential toxic effects. Kidney is considered as such a secondary target organ. However, toxicological information of their effect on renal cells and the mechanisms involved remain sparse. In the present study, the cytotoxicity of nano-SiO_2 of different sizes was investigated on two renal proximal tubular cell lines (human HK-2 and porcine LLC-PK_1). The molecular pathways involved were studied with a focus on the involvement of oxidative stress. Nanoparticle characterization was performed (primary nanoparticle size, surface area, dispersion) in order to investigate a potential relationship between their physical properties and their toxic effects. Firstly, evidence of particle internalization was obtained by transmission electron microscopy and conventional flux cytometry techniques. The use of specific inhibitors of endocytosis pathways showed an internalization process by macropinocytosis and clathrin-mediated endocytosis for 100 nm nano-SiO_2 nanoparticles. These nanoparticles were localized in vesicles. Toxicity was size- and time-dependent (24 h, 48 h, 72 h). Indeed, it increased as nanoparticles became smaller. Secondly, analysis of oxidative stress based on the assessment of ROS (reactive oxygen species) production (DHE, dihydroethidium) or lipid peroxidation (MDA, malondialdehyde) clearly demonstrated the involvement of oxidative stress in the toxicity of 20 nm nano-SiO_2. The induction of antioxidant enzymes (catalase, GSTpi, thioredoxin reductase) could explain their lesser toxicity with 100 nm nano-SiO_2.

1. Introduction

The rapid development of nanotechnology has led to an increase in the number of manufactured products containing materials at the nano-scale. Nanomaterials are commonly defined as materials with one dimension of less than 100 nm. As silica nanoparticles (nano-SiO_2) are among the top five commonly used nanomaterials listed in the nanotechnology consumer products by the Woodrow Wilson International Center for Scholars (Hansen et al., 2008), special attention must be paid to their toxicity (Chen et al., 2004; Fuller et al., 2008). Indeed, their potential effects on human health due to their particular physico–chemical properties could be different from those at macro-scale.

Studies on the biological effects of nanoparticles are often focused on pulmonary toxicity. In fact, nanoparticles can easily disperse into the air due to their very low density, and their inhalation may cause lung damage. Following the process of translocation across biological barriers, nano-SiO_2 can be transported into the blood and deposit in target organs where the nanoparticles exert potential toxic effects (Fruijtier-Polloth, 2012). Kidney could be a target because of its role in elimination of xenobiotics. Indeed, nano-SiO_2 (45 nm) were exhibited prominent distribution in liver, urinary bladder and kidney after intravenous injection of in mice (He et al., 2008). Cho et al. (2009) demonstrated that SiO_2 nanoparticles with a size of 50 and 100 nm were cleared in urine. Moreover, some inorganic nanoparticles such as copper nanoparticles are deposited mainly in liver, spleen and kidney (Chen et al., 2006). Swollen glomeruli and massive renal tubule necrosis are observed in exposed mice (Chen et al., 2006) with presence of proteinic liquid in renal tubule containing copper. Similarly, free cadmium are accumulated in kidney of Sprague Dawley rats after intraperitoneal injection but intact nanoparticles were also detected, with a level in these organs which increases with doses (Arslan et al., 2011). A greater

* Corresponding author at: Pharmacochimie, FRE3396, University Bordeaux Segalen, College of Pharmacy, Department of Toxicology, 146 rue Léo SAIGNAT, 33076 Bordeaux Cedex, France. Tel.: +33 0557 571 245; fax: +33 0557 571 244.
E-mail addresses: isabelle.passagne@u-bordeaux2.fr (I. Passagne), marie.morille@inserm.fr (M. Morille), marine-rousset@hotmail.fr (M. Rousset), igor.pujalte@etud.u-bordeaux2.fr (I. Pujalté), beatrice.lazou@u-bordeaux2.fr (B. L'Azou).

0300-483X/$ – see front matter © 2012 Elsevier Ireland Ltd. All rights reserved.
http://dx.doi.org/10.1016/j.tox.2012.05.010

amount of intact nanoparticles are observed than that of free cadmium. Acute toxicity with kidney injuries is also obtained with TiO_2 (titanium dioxide) nanoparticles in mice after oral or intraperitoneal administration (Wang et al., 2007; Chen et al., 2009).

Silica is a compound that can be divided into crystalline or amorphous molecular structures. Previous studies already showed that chronic inhalation of the crystalline form may cause fibrosis and cancer (IARC, 1997; Cocco, 2001; Cocco et al., 2007). Similarly, exposure to amorphous silica at the micro-scale has led to systemic sclerosis, rheumatoid arthritis and chronic renal diseases. Indeed, Silica particles are known to induce nephropathy in workers by an indirect and direct toxic effect via deposition of particle in the renal parenchyma (Steenland et al., 2002). In a recent study, nano-SiO_2 induced pulmonary and cardiovascular damage with atrio-ventricular blockage and ischemic disorders, notably in old rats (Yang et al., 2010). Particle size may be a major factor in the toxicity of nanoparticles. No effect was observed in BALB/c mice at 100 mg/kg with 300 nm or 1000 nm nano-SiO_2 whereas acute and chronic liver damage occurred already at 30 mg/kg with 70 nm nano-SiO_2 (Nishimori et al., 2009). Nanoparticles may have biological effects that are different and more severe than micrometer-sized particles.

The mechanism by which nano-SiO_2 induce toxicity is poorly understood. However, numerous studies have reported that oxidative stress is an important mechanism of toxicity for other nanoparticles (Marano et al., 2010; Moller et al., 2010). The formation of reactive oxygen species (ROS) can be regarded as the possible mechanism responsible for the toxicity since the crystalline silica has been described as causing oxidative stress and inflammatory response (Castranova, 2004; Antognelli et al., 2009; Akhtar et al., 2010). Under normal biological conditions, the human organism develops cellular defense mechanisms such as catalase to reduce ROS level. However, when the ROS production is great, various events like lipid peroxidation are initiated and lead to cellular dysfunction or death. Previously, Shang et al. (2009) showed that hydroxyl radical generation after nano-SiO_2 exposure, is size-dependent. Some authors also suggest a possibly size-dependent genotoxic effect of silica nanoparticles (Gonzalez et al., 2010). In fact, 16 nm nano-SiO_2 induces a greater formation of micronucleus than 60 nm and 104 nm nano-SiO_2.

The aim of this study was to evaluate the cytotoxicity of amorphous nano-SiO_2 and investigate possible mechanisms of toxicity. The establishment of a relationship between physicochemical properties and toxic effects requires information on size distribution, surface area and charge. Among these parameters, particle size plays an important role in their biological reactivity. To investigate the influence of size, the toxicities of nano-SiO_2 with sizes of 20 nm and 100 nm were assessed in renal cells. Proximal tubular cells (human HK-2 or porcine LLC-PK_1) were selected to determine the possible nephrotoxicity of nano-SiO_2. Indeed, there are only few study on toxic effects induced in renal cells. The impact of oxidative stress in inducing cell death by nanoparticles was assessed by measuring the production of ROS or the induction of antioxidant enzymes such as thioredoxin reductase or catalase. Another objective was to compare the penetration mechanisms of nano-SiO_2. To explore the kinetics and mechanisms of the cellular uptake (endocytosis or macropinocytosis) of nano-SiO_2 with surface coatings, we used flow cytometry analysis. In addition, the localization of nanoparticles in cells was examined by transmission electron microscopy (TEM). These findings provide additional information in understanding the cytotoxicity of nano-SiO_2 on renal cells.

2. Material and methods

2.1. Chemicals

All chemicals were from Sigma–Aldrich (St. Louis, MO, USA) unless stated otherwise. Dihydroethidium (DHE) for ROS measurement was from Fluka Chimie (Buchs, Switzerland). WST-1 was purchased from Roche Diagnostics (Meylan, France). Polystyrene latex beads for fluorescence microscopy were from Sigma Aldrich (St-Quentin-Fallavier, France). Trizol® reagent, oligo-dT primer, MLV-reverse transcriptase and PCR (Polymerase Chain Reaction) reagents were obtained from Invitrogen (Carlsbad, CA). All products used for cell culture were purchased from Lonza (Verviers, Belgium), except fetal calf serum (Eurobio, Les Ullis, France).

2.2. Nanoparticles

The SiO_2 (nano-SiO_2) nanoparticles were synthesized using the reverse microemulsion process invented by Dr. A. Auger (CEA Grenoble, Department of Nano Materials, France) (Auger et al., 2011). Two nano-SiO_2 were selected for this study: fine SiO_2 (100 nm) and ultrafine SiO_2 (20 nm). To explore penetration mechanisms of nano-SiO_2 using flow cytometry, nanoparticles (100 nm) labeled with the fluorochrome TMPyP (5,10,15,20-tetrakis-(1-methyl-4-pyridino)porphyrin tetra(toluene-4-sulafonate)) were synthesized. Before all experiments, all nanoparticles were sonicated (20 s, 3 times at 60 W) (Vibracell 75186, 130 W, 56–60 Hz) to prevent agglomeration. For in vitro toxicity testing, the nanoparticles were extemporaneously dispersed in RPMI 1640 medium without serum or red phenol and the nominal dose was used, because this is the most appropriate metric as previously described (Lison et al., 2008).

2.3. Characterization of silica nanoparticles

Characterization of nanoparticles is an important step before each toxicological study (Powers et al., 2006). Transmission Electron Microscopes (TEM JEOL 2000FX and FEM JEOL 2200FS with Field Emission Microscope) were used to evaluate distribution of size, shape and aggregation state from SiO_2 nanoparticles with an SIS image acquisition system. Nanoparticles were sonicated (20 s, 3 times at 60 W) and diluted in ultrapure deionized water. Nano-SiO_2 suspension was deposited on collodion-coated carbon grids and was allowed to dry at ambient temperature before analysis by electron microscopy. The size distribution was determined after analysis of a particle number $\geq$150. Element analysis was performed by energy dispersive X-ray spectrometer (EDS coupled with TEM and FEM) to confirm the composition of nano-SiO_2, as compared to the spectral database of the wavelength emitted. The average hydrodynamic diameter by dynamic light scattering (DLS) measurement, the polydispersity index (Pdl) and the zeta potential were determined using a Malvern Zetasizer® (Nano Series DTS 1060, Malvern Instruments S.A., Worcestershire, UK). A polydispersity index above 0.3 indicated a broad distribution. Turbidimetry was measured to characterize particle dispersion rates in RPMI 1640 serum-free medium or in ultrapure deionized water using an HACH 2100AN turbidimeter. This method quantifies the degree to which light traveling through a sample is scattered by the suspended particles. Results were expressed in Nephelometric Turbidity Units (NTU).

2.4. Cell culture

Human kidney (HK-2) cells were purchased from the American Type Culture Collection (ATCC, CRL-2190). HK-2 cells possess functional characteristics of human proximal tubular epithelium (Ryan et al., 1994). HK-2 cells were cultured in DMEM F-12 medium supplemented with 10% heat-inactivated fetal calf serum, 1% L-glutamine (2 mM), 1% penicillin (100 μg/ml)/streptomycin (100 U/ml). Porcine tubular LLC-PK_1 cells derived from the Hampshire pig were purchased from the European Collection of Cell Cultures (ECACC). Cells were grown in EMEM (Eagles Minimum Essential Medium) supplemented with 5% heat-inactivated fetal calf serum, 10 mM Hepes, 2 mM L-glutamine, streptomycin (100 U/ml) and penicillin (100 μg/ml). All cell lines were maintained at 37 °C in a 5% CO_2 humidified atmosphere.

2.5. Cellular uptake

Briefly, cells were grown on glass slides until reaching sub-confluence and then exposed to nano-SiO_2 for 24 h at 10 μg/ml and 25 μg/ml for 20 nm or 100 nm nano-SiO_2 respectively. The medium was removed gently and cells were washed twice with PBS (Phosphate Buffered Saline) and fixed by 2.5% (v/v) glutaraldehyde in 0.045 M sodium cacodylate buffer for 2 h at 4 °C. After incubation, post-fixation was performed in 1% osmium tetroxide (pH 7.4) for 2 h at ambient temperature. The cells were scraped off and washed with sodium cacodylate buffer. Samples were dehydrated in ascending grades of ethanol and embedded in epoxy resin. The ultrathin sections (60 nm) were obtained using an ultramicrotome and then were mixed in solutions of uranyl acetate and lead citrate. Before observation, the sections were rinsed with water and dried. Morphologic characteristics of cells were observed with a Hitachi H7650 Transmission Electron Microscope (TEM) under an

accelerating voltage of 80 kV (BIC, Bordeaux Imaging Center, University Bordeaux Segalen), and digital images were obtained with a Gatan camera (ORIUS 11MPxl).

2.6. Internalization study by flow cytometry

Changes in cell granularity due to uptake of particles can be directly assessed by measuring the increase in scattering (SSC, side scatter) of the laser light in a flow cytometer. It has previously been shown that cell fluorescence after phagocytosis of fluorescent latex beads increases in the same manner as the mean SSC of the cells (L'Azou et al., 2008). First, we checked particle internalization by LLC-PK_1 and HK-2 cells using fluorescent latex beads (30 nm). To investigate the endocytic processes involved in internalization, an uptake assay of fluorescent nano-SiO_2 (100 nm) was performed by flow cytometry in the presence of compounds known to inhibit specific pathways of endocytosis. Initially, we used the WST-1 assay to verify that the fluorescent labeling had not induced changes in toxicity. To study endocytosis, cells (0.6×10^6/ml) were plated in 12-well cell microtiter plates and then allowed to grow at 37 °C. After 48 h, cells were rinsed with RPMI 1640 serum-free medium without phenol red and then treated in the same medium with endocytosis inhibitors at a toxic concentrations: chlorpromazine (10 mM), cytochalasin D (10 μg/ml), dynasore (80 μM), filipin (1.5 μM), methyl-β-cyclodextrin (10 mM), genistein (200 μM) or nystatin (3 μg/ml), for 1 h at 37 °C without nanoparticles. The media were then changed to fresh media containing the inhibitors and nanoparticles (25 μg/ml), and further incubated at 37 °C for 4 h. Labeling of the 100 nm nanoparticles with porphyrin (nano-SiO_2 porphyrin) allowed us to monitor the internalization by cytometry (λ_{ex} = 422 nm; λ_{em} = 666 and 718 nm). After incubation, cells were washed twice with Hanks Balanced Saline Solution (HBSS) and harvested by trypsin–EDTA. Cell pellets were washed three times in HBSS and were finally fixed in 1% formaldehyde/azide/PBS. Experiments were carried out at 4 °C in order to certify that the mechanism involved is an active transport pathway (Mamdouh et al., 1996; Muller et al., 2006; dos Santos et al., 2011). Analysis of internalized nanoparticles was performed with a BD FACS Canto™ fluorescent-activated flow cytometer running on BD FACS Diva™ software (BD Biosciences). Cell profiles were constructed on the basis of granularity (side scatter) and size (forward scatter). A region was gated, thus isolating and selecting living cells from unphagocytosed nanoparticles and dead cells. A total of 10,000 events were analyzed for each sample and experiments were performed in triplicate. The fluorescence value of cells alone was defined as negative control and this value was subtracted from all other values (cells without nanoparticles). The value obtained for internalization of nano-SiO_2 porphyrin was considered as the positive control (100% uptake). To assess endocytosis inhibitors, results were normalized to the positive control (nano-SiO_2 porphyrin without inhibitor).

2.7. Cytotoxicity assays

The effects of SiO_2 nanoparticles on HK-2 and LLC-PK_1 cells were determined by WST-1 and clonogenic assays as previously described (Passagne et al., 2003; Pujalte et al., 2011).

The WST-1 assay evaluates cellular mitochondrial activity. It is based on cleavage of the tetrazolium salt to a soluble formazan dye by succinate-tetrazolium reductase, a mitochondrial enzyme that is active only in viable cells. Briefly, cells were seeded into 96-well microtiter plates at 5000 or 20,000 cells per well for LLC-PK_1 and HK-2 cells respectively. Cells were exposed to different concentrations of nano-SiO_2 ranging from 5 μg/ml to 500 μg/ml (in 100 μl RPMI 1640 serum-free medium per well, six wells per concentration level) at 37 °C for different exposure times (24 h, 48 h, 72 h). After exposure, cells were washed with RPMI 1640 serum-free medium and incubated in 100 μl RPMI 1640 serum-free medium containing WST-1 solution (10 μl/well). Absorbance at 450 nm was measured using a photometer (Labsystems Multiscan MS) with a reference wavelength of 630 nm. The effect of nano-SiO_2 on cell survival was expressed as the percentage of cell viability in relation to that of untreated cells and IC_{50} (concentrations inhibiting growth by 50%) were obtained from cytotoxicity curves.

The clonogenic assay determines the ability of cells to form colonies after toxic treatment. Contrary to the WST-1 assay, it has the advantage of not using a colorimetric indicator dye. In fact, nanomaterials are known to interact frequently with the colorimetric indicator used in cytotoxicity assays. Briefly, cells were plated at a density of 10^6 cells in 75 cm^2 flasks. Cells were then treated with nano-SiO_2 at various concentrations for 24 h. These concentrations were chosen according to the IC_{50} values obtained by the WST-1 assay. The doses tested were 5 μg/ml, 10 μg/ml and 25 μg/ml for LLC-PK_1 cells versus 25 μg/ml, 50 μg/ml and 100 μg/ml for HK-2 cells. Experiments with 50 μg/ml nano-SiO_2 (20 nm) in LLC-PK_1 were not undertaken because of the loss of their capacity to adhere to culture plates. Next, the medium was replaced by fresh medium for 16 h. Then, the cells were replated at 3000 and 10,000 cells per 60 cm^2 in a Petri dish for LLC-PK_1 and HK-2 respectively. Cell colonies were stained 10–12 days later with Giemsa and counted automatically using Bio1D® image analysis software (Vilber Lourmat, France). The loss of colony-forming ability was expressed as a percentage relative to untreated cells.

2.8. Reactive oxygen species (ROS) assay

Superoxide radicals were detected with the fluorescent probe dihydroethidium (DHE). In cells, DHE reacts with superoxide anion to form ethidium, which exhibits red fluorescence. Briefly, subconfluent HK-2 or LLC-PK_1 cells were exposed for 24 h to different concentrations of nano-SiO_2 and were then incubated with 5 μM DHE in HBSS (2 mM $CaCl_2$, 1 mM $MgSO_4$) at 37 °C for 30 min. At the end of incubation, cells were scraped off and cell suspension was sonicated. After centrifugation, supernatants were collected and fluorescence was measured using a fluorimeter (Kontrol Instrument, SFM 25, Eching, Germany) at excitation wavelength 488 nm and emission wavelength 512 nm. Hydrogen peroxide solution served as positive control for cellular ROS induction. For each sample, $O_2^{\bullet -}$ production was expressed as mean fluorescence ratio (fluorescence of exposed cells/fluorescence of control cells) from the same experiment. Data were obtained from at least 3 independent triplicates.

2.9. Lipid peroxidation assay

Malondialdehyde (MDA) formed (as a product of lipid peroxidation) was evaluated using the thiobarbituric acid reactive species (TBARS) assay (Wang et al., 2009b). This method is based on the quantification of colored complex formed between thiobarbituric acid (TBA) and MDA after acid hydrolysis reaction. Briefly, nano-exposed cells were collected by scraping into water and 1% Triton-X100 was added to each sample. 500 μl of cell extract were mixed with 500 μl of hydrolysis solution (0.25 M HCl containing 3.75% (v/v) TBA and 15% (v/v) trichloroacetic acid) and incubated at 90 °C for 60 min. After cooling in ice to stop hydrolysis, the complex formed was extracted with 1 ml of *n*-butanol. The mixture was vigorously shaken and centrifuged at $3000 \times g$ for 10 min. The absorbance in butanolic phase was measured using a fluorimeter at excitation wavelength 532 nm and emission wavelength 553 nm. Cadmium chloride ($CdCl_2$) solution served as positive control for induction of lipid peroxidation. The results were calculated as micromole of malondialdehyde per mg of protein and data were expressed as a ratio in relation to the control group. Protein concentration was determined in cell lysate by the Bradford method (Bradford, 1976).

2.10. Antioxidant gene expression

After exposure to nano-SiO_2, the expression of some antioxidant genes was studied in human HK-2 cells using standard procedures of Polymerase Chain Reaction (PCR). Briefly, extraction of total cellular RNA was obtained using Trizol® reagent according to the manufacturer's procedure. Reverse transcription was carried out using 2 μg of total RNA at 37 °C for 1 h with 1 μg oligo-dT primer and 5U MLV-Reverse Transcriptase. cDNA amplification was performed using human specific primers whose sequences are shown in Table 1. Oxidative stress-associated genes was studied: catalase, thioredoxine reductanse and GSTpi (glutathione S-transferase). Actin mRNA was also amplified as a loading control. Amplified products were separated on 1% agarose gel supplemented with ethidium bromide, which binds to the double-stranded DNA. PCR products were visualized by ultraviolet illumination and band intensities were quantified by densitometry analysis using Image J software.

2.11. Statistics

Nanoparticle size (mean ± SD) obtained by TEM using ImageJ software was calculated by measuring over 100 nanoparticles in random fields of view. For the cytotoxicity WST-1 experiment, % of cellular viability was calculated using the formula (absorbance treated sample × 100/absorbance control sample) and expressed as mean ± SE of at least three triplicate independent experiments. Non-linear Boltzman regression analysis was performed using the Origin® software (Origin Lab. Corp., Northampton, USA) for IC_{50} (defined as concentration which induces 50% cell mortality increase). For capacity of forming colony, ROS and MDA production, statistical analysis was performed for the experiments conducted in at least triplicate using the student test. Concerning study of endocytosis, the Dunnett test was used for statistical analysis. For all experiments, results with $p < 0.01$ (**) and $p < 0.05$ (*) were considered to be statistically significant.

3. Results

3.1. Characterization of silica nanoparticles

As the interaction between SiO_2 nanoparticles and the biological system may depend on particle diameter or zeta potential, we characterized these physico-chemical properties of the different SiO_2 used in this study, as recommended for toxicological evaluation (Powers et al., 2006). To determine particle size distribution, we first observed nano-SiO_2 under a JEOL 2200FS FEM microscope (Figs. 1A and 2A). Silica nanoparticles appeared spherical, well dispersed and not altered. Element analysis by energy

Table 1
PCR primers, amplicon size, temperature of hybridization and number of amplification cycles.

Genes	Direction	Primer sequences (5′→3′)	Hybridization temperature (°)	Amplicon size (pb)	Number of cycles
β-Actin	Forward Reverse	GGCATCGTGATGGACTCCG GCTGGAAGGTGGACAGCGA	57	613	23
Catalase	Forward Reverse	TCGACCCAAGCAACATGCCA ACGCTAAGCTTCGCTGAA	56	621	34
GSTPi	Forward Reverse	CTCACTCAAAGCCTCCTGCCTAT CAGGATGGTATTGGACTGGTACAG	60	85	35
Thioredoxine reductase 1	Forward Reverse	AACCACTGGCTCGTTCCGT GCTGGAAGGTGGACAGCGA	58	692	35

dispersive X-ray spectrometer (EDS coupled to TEM) confirmed the composition of all nano-SiO_2 (Figs. 1B and 2B). As shown in Figs. 1C and 2C, primary diameter of nanoparticles were calculated with a Transmission Electron Microscope fitted with a camera and using ImageJ software. The 20 nm nano-SiO_2 had a size distribution around 15 or 20 nm (Fig. 1D) with a mean of 16.25 ± 3.02 (Table 2). Concerning 100 nm nano-SiO_2 (Fig. 2D), the average particle size was 85.69 ± 15.32 nm (Table 2). These findings were in accordance with the information given by the supplier (Dr. A. Auger; CEA Grenoble, Department of Nano Materials, France). TEM provided information on the primary diameter of nanoparticles under dryness and not under experimental conditions (in RPMI 1640 serum-free medium). To closely work under experimental conditions, average hydrodynamic diameters were determined with particles suspension in medium by DLS. As shown in Table 2, the average hydrodynamic diameter of 100 nm nano-SiO_2 was equal to the primary diameter size obtained previously, with 99 ± 3 nm for 100% of the particles in RPMI 1640 serum-free medium samples and a polydispersity index of 0.201. By contrast, the average hydrodynamic diameter obtained for nano-SiO_2 (20 nm) was larger than the TEM values and the size distribution was more heterogeneous, with 31% of nanoparticles having a size of 19 ± 6 nm and 69% a size of 52 ± 14 nm, associated with a high polydispersity index (0.538). These results suggest the slow formation of aggregates in RPMI

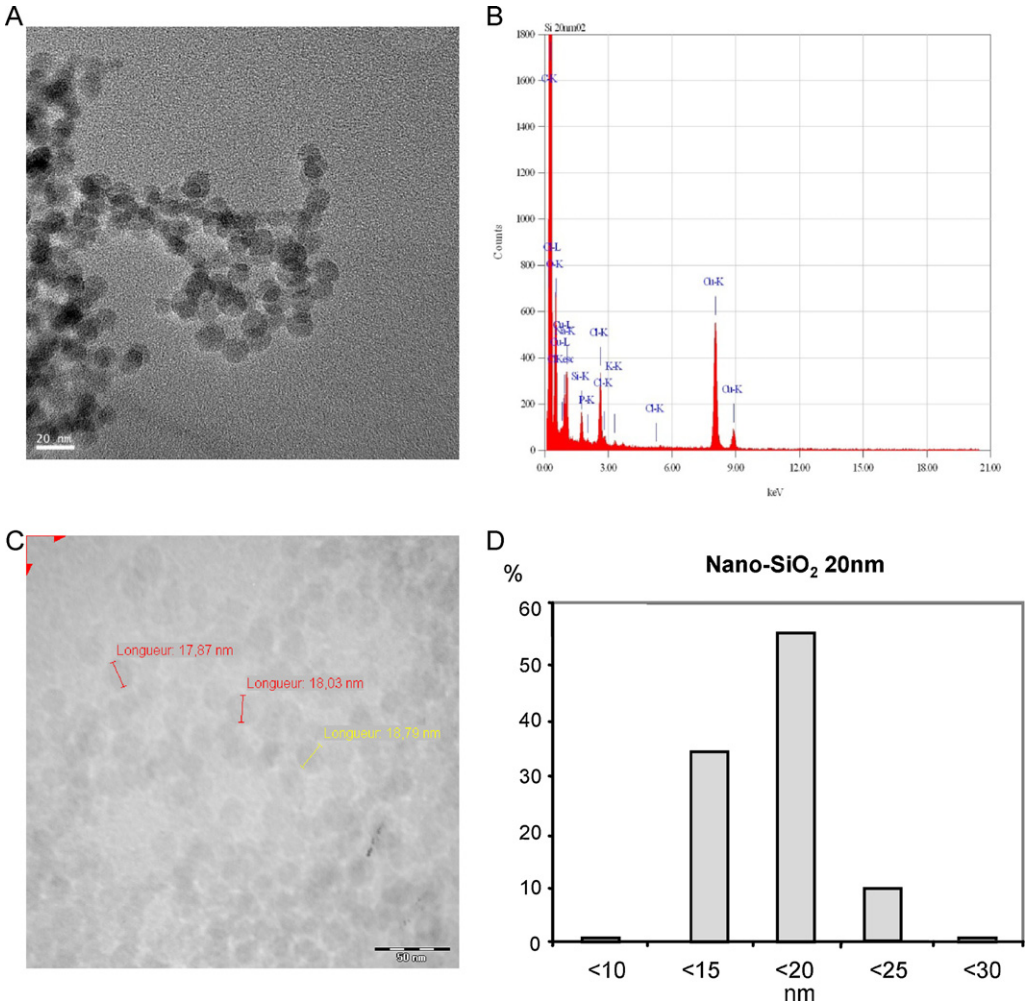

Fig. 1. Characterization of 20 nm nano-SiO_2. Images obtained by JEOL 2200FS with Field Emission Microscope (FEM) (A), element analysis by energy dispersive X-ray spectrometer (B), size analysis (C) by JEOL 2000 Transmission Electron Microscope (TEM) and the corresponding histogram of particle size distribution (D), as described in Section 2. Images were taken at 250 K (A) and 200 K (C).

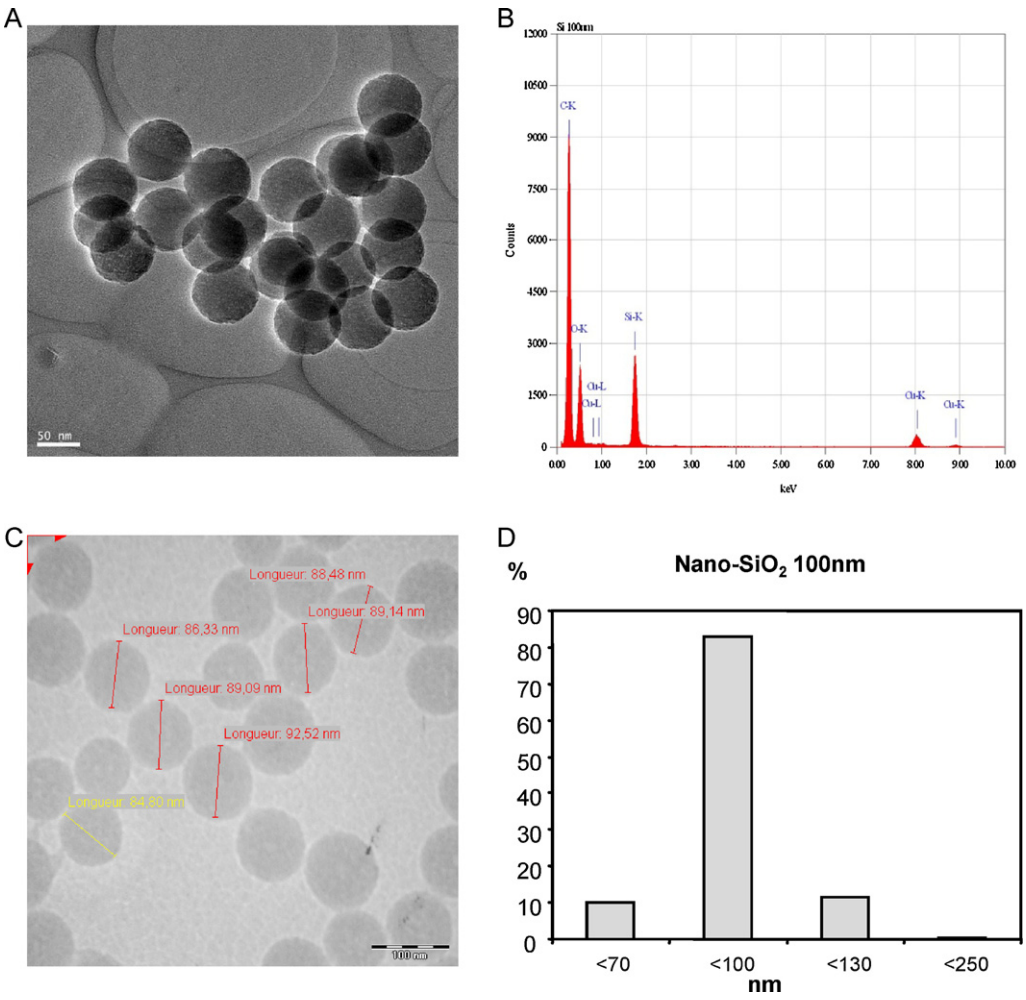

Fig. 2. Characterization of 100 nm nano-SiO_2. Images obtained by JEOL 2200FS with Field Emission Microscope (FEM) (A), element analysis by energy dispersive X-ray spectrometer (B), size analysis (C) by JEOL 2000 Transmission Electron Microscope (TEM) and the corresponding histogram of particle size distribution (D) as described in Section 2. Images were taken at 60 K (A) and 55 K (C).

1640 serum-free medium. This moderate effect of aggregation is similar to that obtained in a previous study with smaller nanoparticles (10 nm) (Waters et al., 2009). The nanoparticles were also characterized in terms of surface charge. These nano-SiO_2 have a negative surface charge, with zeta potential values of -45 ± 1.3 mV and -52 ± 1.8 mV, for 20 nm and 100 nm nano-SiO_2 respectively. This high negative potential contributes to the absence of particle aggregation in suspension via repulsive forces. Additionally, dispersion was assessed by turbidimetry. Low values were obtained with 20 nm and 100 nm nano-SiO_2 reflecting good dispersion of nanoparticles in RPMI 1640 serum-free medium (Table 2). As spherical shapes of nanoparticles were confirmed by TEM, the specific surface area was calculated from the diameter as measured by the following equation (Powers et al., 2006; Nabeshi et al., 2011):

$$\text{SSA} = \frac{6}{d \times p}$$

(SSA is the specific surface area (m^2/g); d is the diameter (mm); p is the density (g/cm^3)).

Table 2
Physico-chemical characteristics of silica nanoparticles.

Particles	Primary diameter[a] (nm)	Average hydrodynamic[b] diameter (nm)	Specific surface area (m^2/g)	Zeta potential (mV)	Aggregates[c]	Turbidimetry[d] (NTU)	Cristal structure
20 nano-SiO_2	16.25 ± 3.02	19 ± 6 (31%) 52 ± 14 (69%)	168	−45 ± 1.3	No aggregate	6.3 ± 0.9 (water)* 11.0 ± 3.1 (water)** 5.3 ± 1.7 (RPMI)* 11.8 ± 3.8 (RPMI)**	Amorphous
100 nano-SiO_2	85.69 ± 15.32	99 ± 3 (100%)	31.8	−52 ± 1.8	No aggregate	3.0 ± 0.3 (water)** 4.8 ± 0.9 (water)** 4.3 ± 0.3 (RPMI)* 8.3 ± 0.6 (RPMI)**	Amorphous

[a] Diameter determined in deionized water by TEM (Transmission Electron Microscope).
[b] DLS measurement in RPMI 1640 serum-free medium.
[c] Aggregation state determined by TEM (Transmission Electron Microscope).
[d] Turbidimetry measurements performed in water or RPMI 1640 serum-free medium at 25 μg/ml (*) and 50 μg/ml (**) to evaluate particle dispersion.

This calculation was based on the primary diameter obtained by TEM and a density of 2.2 g/cm^3 (Fruijtier-Polloth, 2012); for example: $SSA_{20\,nm} = 6/(0.01625 \times 2.2)$. The values of specific surface area were 168.0 m^2/g and 31.8 m^2/g for 20 nm and 100 nm nano-SiO_2 respectively.

3.2. Cellular uptake of silica nanoparticles

The localization of the different nano-SiO_2 in cells was visualized under the TEM microscope. Representative images of LLC-PK_1 cells exposed for 24 h at 20 nm and 100 nm nano-SiO_2 are shown in Fig. 3. Typical images demonstrate that nanoparticles were localized in the cytoplasm after exposure at 20 nm (Fig. 3B and C) or 100 nm (Fig. 3D and E). No localization inside the nucleus or in any other cellular compartment was observed, as shown in Fig. 3B and D. The nuclear membrane of exposed cells was also intact. These nanoparticles are present in vesicles and are dispersed into these vesicles, especially for 100 nm nano-SiO_2. As shown in Fig. 3B and E, nanoparticles had penetrated the LLC-PK_1 cells and did not appear to affect cell morphology as compared to the cell control (Fig. 3A). The experiment with co-incubation of 20 nm and 100 nm nano-SiO_2 led to cytoplasm localization in the same vesicle for these two kinds of nanoparticles, suggesting a similar mechanism of cellular translocation (Fig. 3F). HK-2 cells under the control condition (Fig. 4A) and uptake of nano-SiO_2 (20 nm) are presented in Fig. 4B. Images obtained were difficult to exploit due to the presence of glycogen in many cells, as previously described (Ryan et al., 1994).

3.3. Effect of endocytosis inhibitors on cellular internalization of nano-SiO_2

Because cellular penetration of nanoparticles is an essential prerequisite for toxicity, flow cytometry was used to determine the uptake of nanoparticles, using first fluorescent latex beads. We observed a good correlation between the uptake level and the incubation time (data not shown). Under our experimental conditions, uptake was noticeable after 30 min. A third of the cells (32%) were labeled after 4 h incubation. A concomitant shift in SSC occurred indicating internalization of the beads. The labeling of 100 nm nano-SiO_2 with the fluorochrome TMPyP (λ_{ex} = 422 nm; λ_{em} = 666 and 718 nm) allowed us to study the uptake of nanoparticles by LLC-PK_1 and HK-2 cell lines. In terms of toxicity induced, there was no significant difference between fluorescent nano-SiO_2 and unlabeled controls (data not shown). Various endocytosis inhibitors have been used at appropriate concentrations to block endocytic pathways: cytochalasin D, chlorpromazine, dynasore, genistein, filipin, methyl-β-cyclodextrin and nystatin. Cytochalasin D is commonly reported to be a macropinocytosis inhibitor but can also hinder clathrin- and caveolae-dependent endocytosis. Chlorpromazin and dynasore are known to inhibit clathrin-dependent endocytosis, whereas genistein, filipin, methyl-β-cyclodextrin and nystatin have been extensively used to inhibit clathrin-independent endocytosis, with or without involvement of the caveolae (sphingolipid- and cholesterol-rich microdomains on cell membrane) (Rejman et al., 2004; Macia et al., 2006; Gratton et al., 2008; Roger et al., 2009; Vercauteren et al., 2010).

Fig. 5 represents the internalization of particles by LLC-PK_1 (Fig. 5A) and HK-2 (Fig. 5B) cell lines. When cells were incubated with cytochalasin D, the uptake of nano-SiO_2 was significantly decreased with only 24% and 37% of nanoparticles internalized in LLC-PK_1 and HK-2 cells respectively. Chlorpromazin also induced a strong decrease in internalization in LLC-PK_1 cells (−75%), but the effect was weaker for HK-2 cells (−38%). The effect of dynasore was not significant in either of the cell lines, with a reduction of 7% for LLC-PK_1 versus no inhibition for HK-2 cells. With genistein, no effect was noticed in HK-2 cells (a rise of 35% was even noted), whereas a decrease in uptake was observed in LLC-PK_1 (−50%). Concerning filipin, methyl-β-cyclodextrine and nystatine, uptake was increased to obtain 148%, 115%, and 288% in LLC-PK_1 cells and 162%, 177%, and 188% in HK-2 cells, respectively.

Table 3
IC_{50} values (concentration required to inhibit 50% of cell growth) obtained on LLC-PK_1 and HK-2 cells after exposure to 20 nm or 100 nm nano-SiO_2 (WST-1 assay).

Particles	IC50 (μg/ml) ± SEM		
	Exposure time (h)	LLC-PK_1	HK-2
20 nano-SiO_2	24	66.8 ± 5.0	110.5 ± 17.9
	48	16.9 ± 0.5	58.3 ± 8.2
	72	12.2 ± 1.2	41.8 ± 1.2
100 nano-SiO_2	24	484.7 ± 30.6	>500.0
	48	145.3 ± 20.9	>500.0
	72	81.3 ± 0.3	215.6 ± 7.6

3.4. Cytotoxic effects of silica nanoparticles on renal cells

The cytotoxic effects of nano-SiO_2 on renal cells were first studied by the WST-1 assay using different nanoparticles sizes (20 nm or 100 nm). All nanoparticles reduced cell viability in a dose-dependent manner (Fig. 6). The concentration required to inhibit 50% of cell growth (IC_{50}) was determined from cytotoxicity curves (Table 3). In LLC-PK_1, nano-SiO_2 of smaller size (20 nm) were more cytotoxic than 100 nm nano-SiO_2 with IC_{50} values of 66 μg/ml for LLC-PK_1 approximately, whereas IC_{50} values were 485 μg/ml for 100 nm at 24 h exposure (Fig. 6A). Furthermore, LLC-PK_1 cells were more susceptible to cytotoxic effects induced by nanoparticles as compared to HK-2 (Fig. 6A and B). At 100 μg/ml nano-SiO_2 (20 nm), 76.1% of cell mortality was obtained with LLC-PK_1 versus 50.5% for HK-2. The cytotoxic effects also appeared to be time-dependent (Fig. 6C and D). For example, in LLC-PK_1 cells, the IC_{50} value of 20 nm decreased from 66 μg/ml to 17 μg/ml between 24 h and 48 h (Fig. 6C).

The loss of colony-forming ability was next investigated using the clonogenic assay. Contrary to the WST-1 assay, this test discriminates between cytotoxic (cell kill) and cytotastic (decreased growth rate) effects by combining both assays. Results are expressed as a percentage relative to control cells exposed to the vehicle alone. In agreement with the WST-1 assay, it was found that the colony-forming ability of renal cells was significantly reduced after exposure to 20 nm nano-SiO_2 (Fig. 7). Notably at high concentrations, a large statistically significant reduction in colony-forming ability was observed in HK-2 cells to 20 nm with only 12% of colonies remaining after exposure to 100 μg/ml versus 80% for 100 nm nano-SiO_2 (Fig. 7B). Indeed, the colony number was not dramatically affected by exposure to 100 nm nano-SiO_2 in HK-2 cells but colony size was still reduced. Exposure to 100 nm nano-SiO_2 led to a 29% decrease in the number of colonies formed for LLC-PK_1 at 25 μg/ml (Fig. 7A). Furthermore, LLC-PK_1 cells were highly sensitive to 20 nm nano-SiO_2. No colony could be obtained (data not shown) through a loss of cell adhesion to Petri culture at 50 μg/ml, while a 72% colony-forming capacity was observed with HK-2 cells. In agreement with previous results, the cytostatic effect of nano-SiO_2 evaluated by clonogenic assays seemed to be dose- and size-dependent in the two tubular cell lines.

3.5. Effect of nano-SIO_2 on ROS generation

As oxidative stress may be the mechanism responsible for the toxicity of nanoparticles, we evaluated the ability of nano-SiO_2 to produce ROS in renal cells. DHE, a specific fluorescent probe for $O_2^{\bullet -}$ was used to track ROS generation in LLC-PK_1 (Fig. 8A) and HK-2 cells (Fig. 8B). At all concentrations of 20 nm nano-SiO_2, the

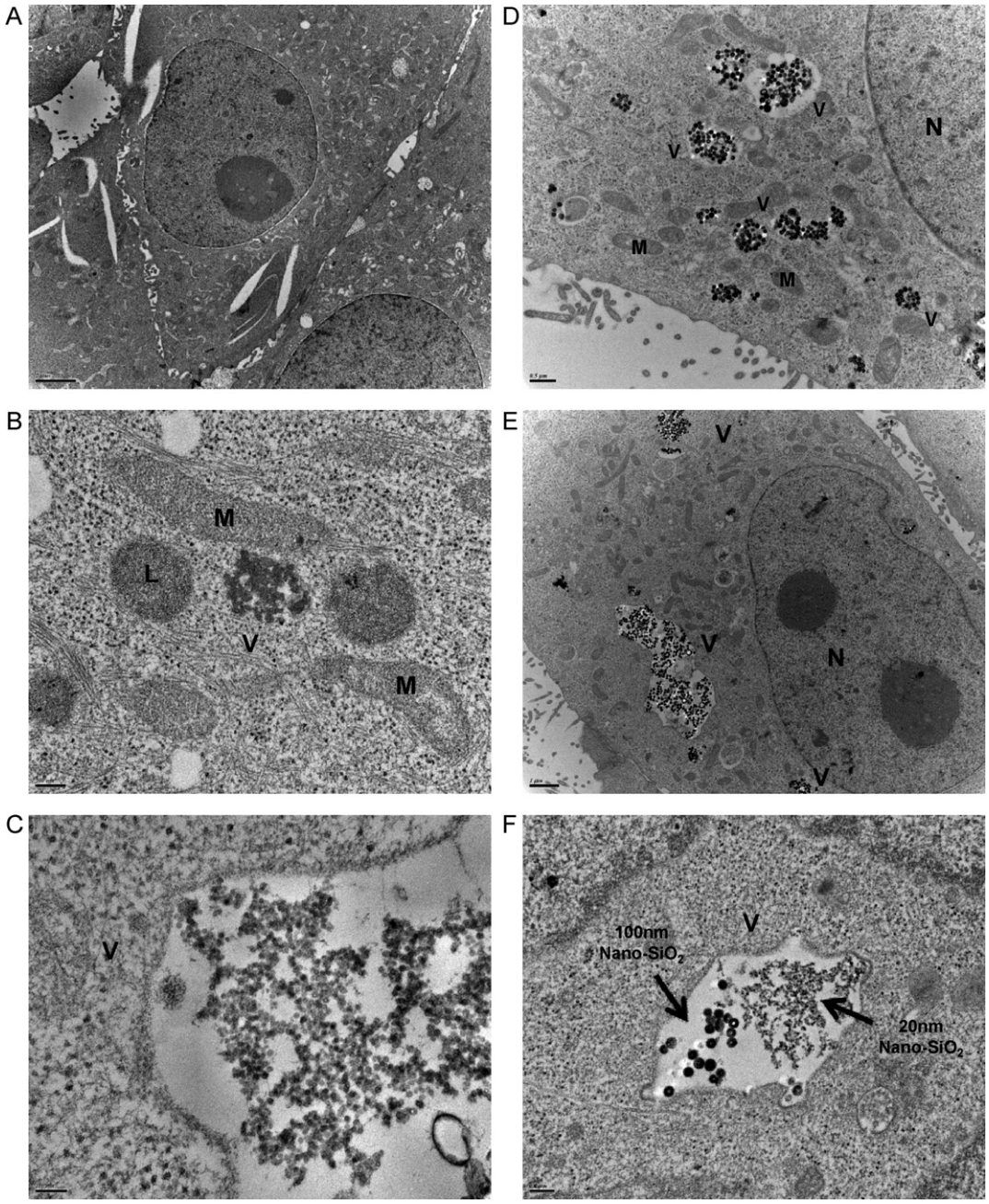

Fig. 3. Observation of nano-SiO_2 uptake using a Hitachi H7650 Transmission Electron Microscope in LLC-PK_1 cells after 24 h incubation without (A) or with various nano-SiO_2: 20 nm (B and C) or 100 nm (D and E). Co-incubation was assessed with the two nanoparticles. A selected image obtained with a Gatan camera (ORIUS 11MPxl) is shown in F. Cell organelles are localized: L (lysosome), M (mitochondria), N (nucleus), V (vesicles).

exposure of LLC-PK_1 cells for 24 h induced a significant increase in fluorescence intensity (compared to control) in a dose-dependent manner, suggesting a stress oxidative phenomenon at 20 nm size (Fig. 8A). The effect of nano-SiO_2 at 100 nm size was different. The $O_2^{\bullet -}$ level was very slightly increased in LLC-PK_1 cells, reaching an increase of 15–20% fluorescence but not in a dose-dependent manner. For concentrations ranging from 5 to 25 μg/ml, the ROS level in HK-2 cells was not significantly altered by 24 h exposure, both for 20 nm and 100 nm nano-SiO_2 (Fig. 8B). A low significant effect was observed at 50 μg/ml on ROS production in HK-2 cells.

3.6. Lipid peroxidation induced by nano-SiO_2

We next examined the amount of MDA formed using TBARS assay because ROS can damage cell membranes and MDA is a major indicator of lipid peroxidation. After LLC-PK_1 exposure for 24 h with 20 nm nano-SiO_2, lipid peroxidation increased sharply in the dose-dependent manner, as shown in Fig. 9A. MDA levels at 25 μg/ml were increased significantly about 2.47-fold for 20 nm nano-SiO_2 versus 1.33-fold for 100 nm compared to that in the control. In HK-2 cells, the value of MDA formed after exposure to 20 nm nano-SiO_2 (25 μg/ml) was similar to that obtained with 100 nm nano-SiO_2, with an increase in ratio compared to control of approximately 1.2 (Fig. 9B).

3.7. Expression of antioxidant genes after exposure to nano-SiO_2

The expression level of some antioxidant genes was studied by RT-PCR (Reverse Transcription-Polymerase Chain Reaction) to evaluate the oxidative stress response of HK-2 cells after nano-SiO_2

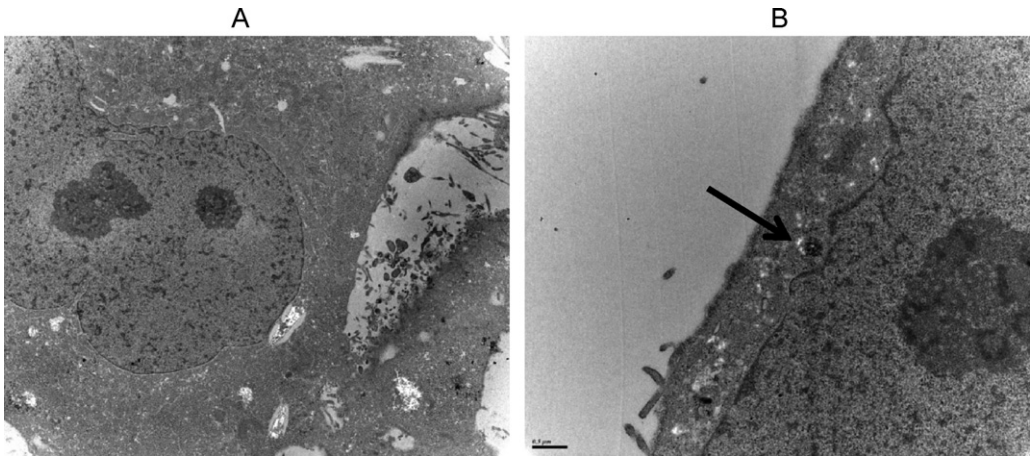

Fig. 4. Cellular uptake of HK-2 obtained with a Hitachi H7650 electron microscope. Representative images are presented for control cells (A) and cells exposed at 20 nm nano-SiO_2 for 24 h. Localization of nanoparticles (↓).

exposure. Agarose gel electrophoresis showed an enhanced mRNA expression of catalase in cells exposed to each nano-SiO_2. As shown in Fig. 10, a maximal induction occurred for catalase gene after 24 h exposure to a high concentration of 20 nm and 100 nm nano-SiO_2 (50 μg/ml). For example, induction increased to a factor of 3.3 versus control at 50 μg/ml of 20 nm nano-SiO_2. In contrast to exposure at 20 nm nano-SiO_2, the level of mRNA thioredoxin reductase was increased gradually in a dose-dependent manner after exposure to 100 nm nano-SiO_2, leading to a highly increased ratio of 2.497-fold at 50 μg/ml. Moreover, a significant induction of GSTpi (1.77-fold) was apparent in HK-2 cells exposed to 100 nm nano-SiO_2 at 50 μg/ml. Therefore, the antioxidant capacity of cells might be solicited especially in the presence of 100 nm nano-SiO_2.

4. Discussion

In this study, proximal tubular (human HK-2, porcine LLC-PK_1) cell lines were used to assess the potential toxicity of silica nanoparticles (nano-SiO_2) on kidney cells and the mechanisms involved in it. Analysis of the mechanism involved was based on the study of

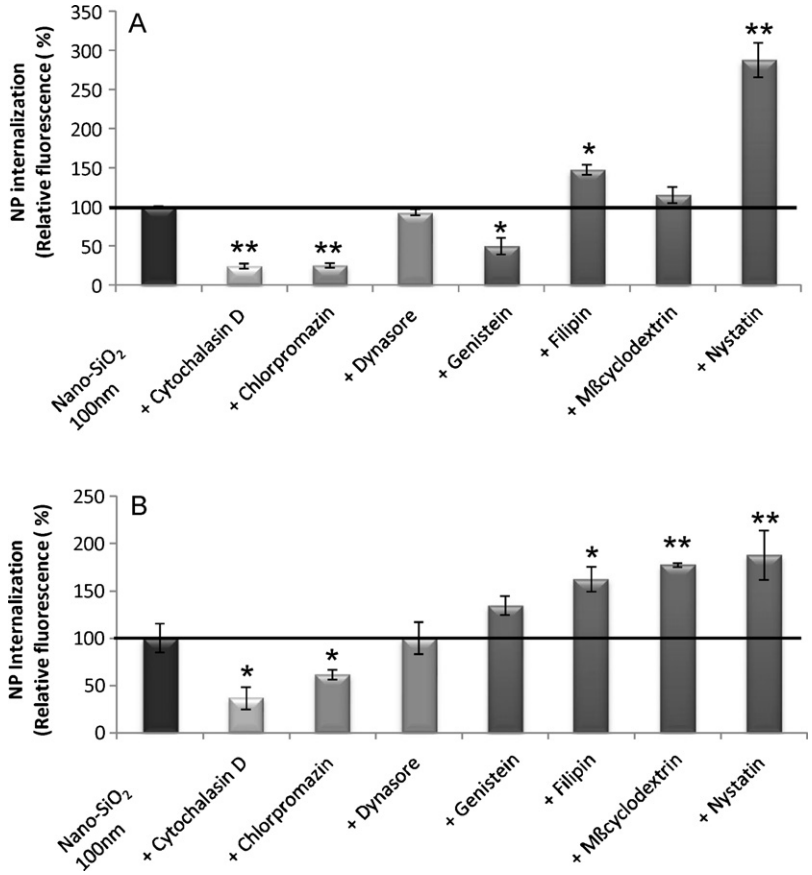

Fig. 5. Study of cellular internalization mechanisms by flow cytometry. Uptake of fluorescent nano-SiO_2 (100 nm) was done in the presence of specific endocytosis inhibitors for LLC-PK_1 (A) and HK-2 (B). Cells were incubated with inhibitors and nano-SiO_2 at 25 μg/ml for 4 h. Percent internalization was normalized to particle internalization without inhibitors. $^{**}p < 0.01$ and $^{*}p < 0.05$ (Dunnett test).

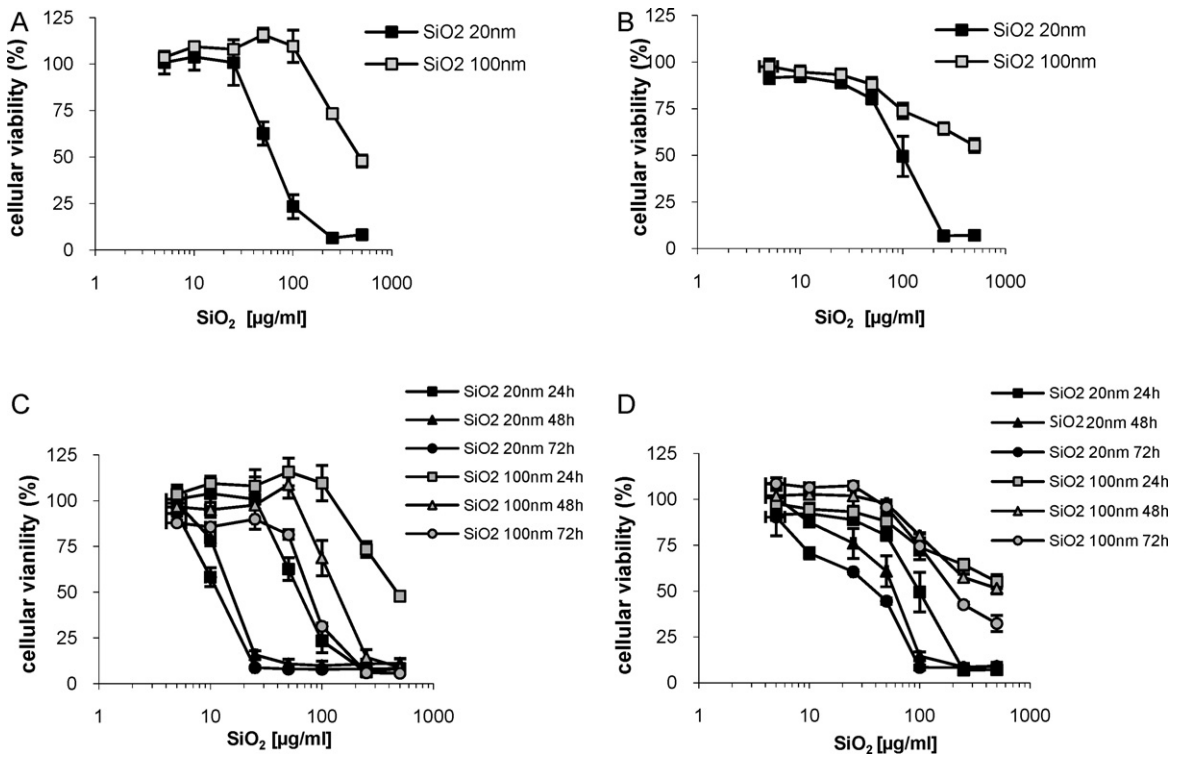

Fig. 6. Effects of nano-SiO_2 on cellular viability of LLC-PK_1 (A) or HK-2 (B) cells after 24 h exposure determined by WST-1 assay. Cells were treated in RPMI serum-free medium with different concentrations of nano-SiO_2 (20 nm or 100 nm). Results are expressed as the percent of cell viability compared to the control. The values presented are the means of three separate experiments ± SEM. Time-dependent cytotoxicity of nano-SiO_2 in LLC-PK_1 and HK-2 cells is represented in C and D respectively.

oxidative stress. The Physico-chemical characterization of nano-SiO_2 showed that these nanoparticles used differ mainly in their size: 20 nm and 100 nm. These nanoparticles, which are amorphous and are considered insoluble in aqueous media, allow us to assess the effect related to nanoparticles and not to the soluble form. The present study demonstrates that nano-SiO_2 are internalized into the cell and localized in the cytoplasm especially. Our findings indicate also that nano-SiO_2 are toxic on kidney cells and that their

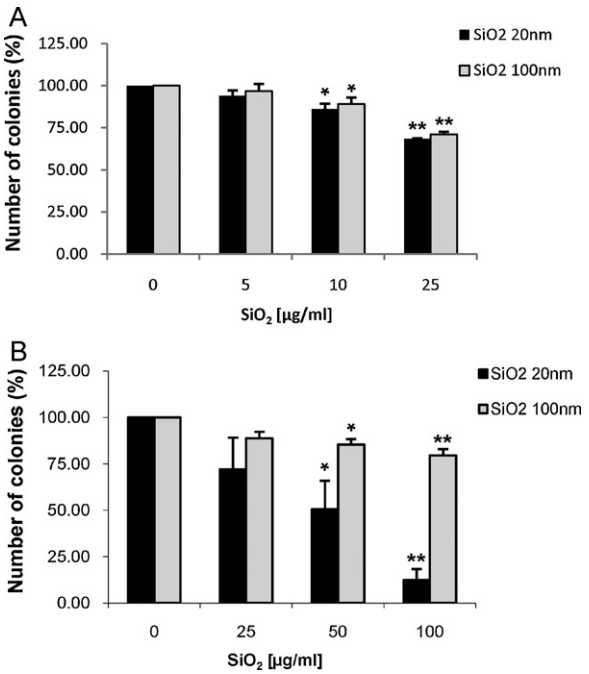

Fig. 7. Effect of nano-SiO_2 (20 nm or 100 nm) on colony formation of LLC-PK1 (A) and HK-2 (B) cells. In clonogenic assay, cells were exposed to increasing concentrations of nano-SiO_2 for 24 h and colony numbers were determined after 10–12 days. Results are expressed as percent of control mean ± SE of three independent experiments. Significance indicated by: $^{*}p < 0.05$ and $^{**}p < 0.01$ versus control cells.

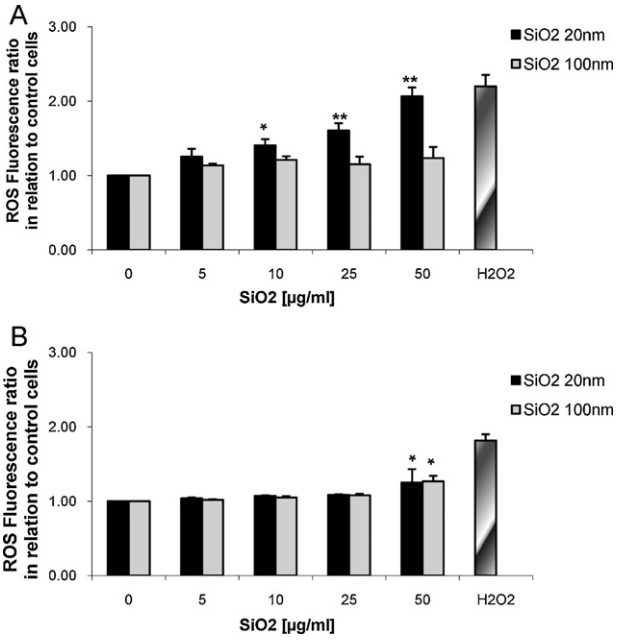

Fig. 8. ROS production induced by nano-SiO_2 in LLC-PK_1 (A) or HK-2 (B) cells determined using DHE (dihydroethidium) probe. Cells were exposed in serum-free medium with different concentrations of nano-SiO_2 for 24 h. Data are expressed as relative fluorescence units in relation to control cells. *Significant difference from control ($^{*}p < 0.05$ and $^{**}p < 0$). The values presented are the means ± SD of at least three independent experiments. H_2O_2 was used as positive control.

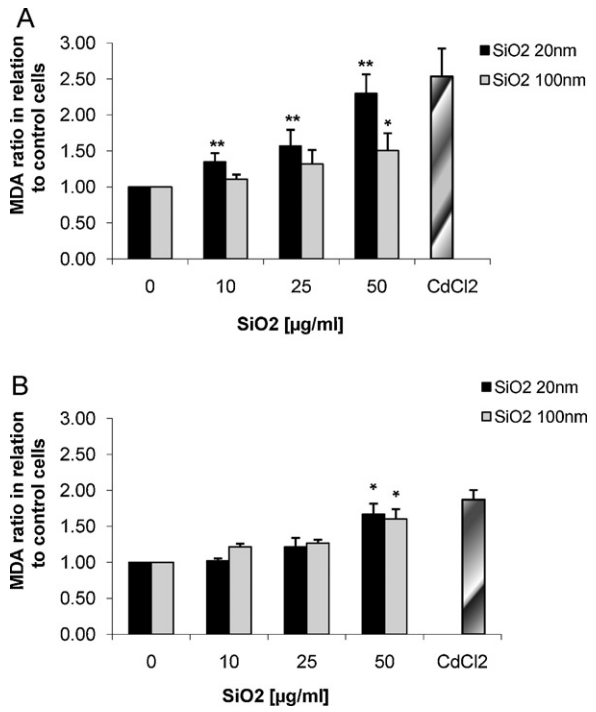

Fig. 9. Detection of lipid peroxidation induced by nano-SiO_2 (20 nm or 100 nm) treatment at different concentrations for 24 h. Cellular MDA levels were assessed by TBARS assay in LLC-PK_1 (A) and HK-2 (B) cells. Data shown are means ± SD ($n = 3$). *Denotes a significant difference from the control ($^*p < 0.05$ and $^{**}p < 0.01$). $CdCl_2$ was used as positive control.

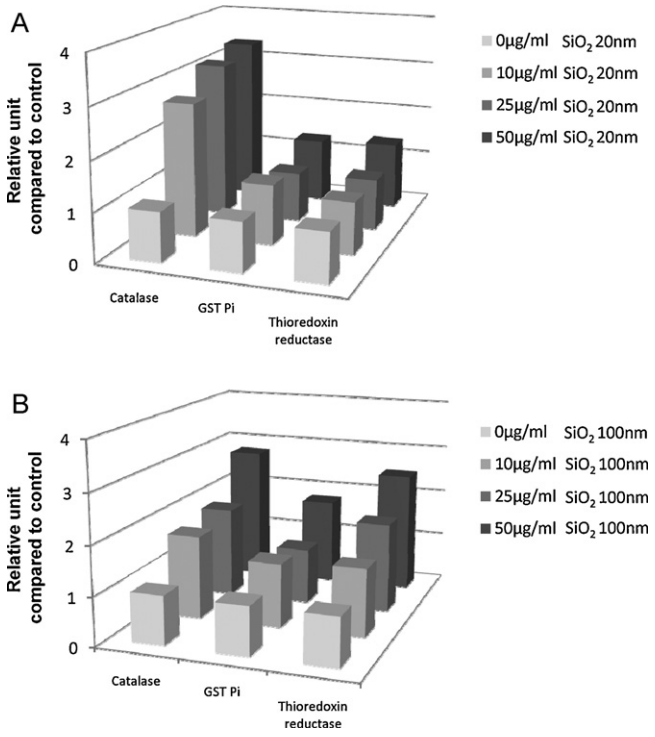

Fig. 10. Expression of antioxidant genes (catalase, GSTpi, thioredoxin reductase) in LLC-PK_1 (A) and HK-2 (B) cells exposed to (20 nm or 100 nm) for 24 h. Densitometric values of gene expression were normalized using actin. Results were presented as a relative units compared to control. Data represent the mean of three individual and independent experiments.

toxicity depends mainly on their size. Cell mortality increased significantly in LLC-PK_1 as their size decreased, with a CI_{50} value 7-fold lower than that at 100 nm. LLC-PK_1 cells are more sensitive than HK-2 cells as previously described with others nephrotoxic xenobiotics (Gunness et al., 2010). The size could be a predictive parameter of the nano-SiO_2 toxicity, as shown in other studies notably in different cells (Lin et al., 2006; Park et al., 2010). Similar results were obtained on human embryonic kidney cells (HEK 293) (Wang et al., 2009a). As in our study, Wang et al. (2009a) reported that cytotoxicity was size- and time-dependent, with 20 nm SiO_2 nanoparticles being more cytotoxic than larger ones (50 nm). It appears that below 30 nm, changes in their structure increase their toxic potential due to variations in surface reactivity (Auffan et al., 2009a). Indeed, for particles larger than 30 nm, fewer than 20% of atoms were localized on the surface whereas at 10 nm, there were approximately 40% of atoms (Auffan et al., 2009b). Moreover, the specific surface area was reduced (about 5-fold) when going from 20 nm to 100 nm. The high toxicity of 20 nm nanoparticles seems to be due to their larger specific surface area that promotes interactions with cells. A recent study on silica toxicity confirmed the influence of surface area and not the state of aggregation (Rabolli et al., 2011). When aggregates are small, the characteristics of nanoparticles are maintained (i.e. surface area). Size, surface area and microporosity have been described to influence toxicity of amorphous nano-SiO_2 in other cell models (Rabolli et al., 2010).

Penetration may also influence the toxicity of nanoparticles via penetration facilitated by their small size. In fact, the amount of silica ingested by Langerhans cells increases when particles size decreases (Nabeshi et al., 2010). The intracellular quantity of nanoparticles was well correlated with the greater cytotoxicity of smaller-sized particles (70 nm compared to 300 nm). In our study, the size-dependent toxicity of nanoparticles was confirmed by clonogenic assay, but this test mainly provided additional information. Indeed, the 100 nm nanoparticles mainly induced slower cell proliferation with cell colonies visible but small in size, whereas with smaller nano-SiO_2 (20 nm), there was only a decrease in number of colonies (size preserved).

For a mechanistic point of view, the production of ROS in kidney cells was significantly increased after exposure to silica nanoparticles, notably at 20 nm. As previously described on other cell types, ROS generation is a size-dependent effect (Wang et al., 2009b; Napierska et al., 2010; Ye et al., 2010; Nabeshi et al., 2011; Gong et al., 2012). This effect is also dependent to surface area of nano-SiO_2. Indeed, 20 nm nano-SiO_2 have surface area which is found to be significantly much more important, compared to 100 nm about 5-fold and produced then important oxidative stress in tubular cells compared to 100 nm, suggesting great reactivity surface of 20 nm. High reactivity could lead to toxicity due to important interactions of nanoparticles with biological systems and cellular environment. Moreover, some authors suggest that the size-dependent toxic effect is caused by a different mechanism of ROS generation. In fact, the amount of hydroxyl radical generated in acellular and cellular models is highly dependent on the size with high ROS production with 14 nm compared to 100 nm and 500 nm silica nanoparticles (Shang et al., 2009). Therefore, the toxic effects seem to be triggered by oxidative stress, as evidenced by great anion superoxide production with 20 nm nano-SiO_2. This generation of primary ROS seems to occur through a mechanism that involves NADPH oxidase (Ushio-Fukai, 2006; Nabeshi et al., 2011). After ingestion of xenobiotic into endosomes, the NADPH oxidase is activate and generate ROS (Nabeshi et al., 2011). The anion superoxide formed could lead to the formation of radical hydroxyl, which is more reactive and destructive for cells. This radical hydroxyl induces destruction of membrane structure by peroxidation of unsaturated lipids. This leads to a loss of physiological cellular integrity resulting in cell death. In our study, the increase in ROS level was

associated with a concomitant elevation of malondialdehyde with 20 nm nano-SiO_2, which reflects lipid peroxidation. It has been reported by Wang et al. (2009a) that oxidative stress plays an important role in toxicity of silica nanoparticles on human embryonic kidney cells, relating to particle size. A great amount of ROS was observed with cells exposed to 20 nm compared to 50 nm (Wang et al., 2009a). Furthermore, authors demonstrated a strong correlation ($R^2 = 0.956$) between cell viability decreased and increase of ROS production after exposure to 20 nm silica nanoparticles. In addition, oxygen radicals also resulted in malondialdehyde production after exposure of human embryonic kidney cells to 20 nm (Wang et al., 2009a). In our study, exposure to 100 nm nano-SiO_2 induces anti-oxidant systems such as catalase, thioredoxin reductase or GSTpi. It is well known that ROS generation causes translocation of Nrf-2 transcription factor, which induces expression of antioxidant genes to protect cells. As previously described (Eom and Choi, 2009), translocation of Nrf-2 was described in Beabs-2B (human bronchial epithelial cells) after exposure to porous silica nanoparticles. This phenomenon could explain the low toxicity of our nanoparticles at 100 nm size. For example, GSTpi is an enzyme that catalyzes reactions in order to detoxify peroxidized lipids. In MRC-5 cells (human lung fibroblast) exposed to nano-SiO_2, an enhancement of the specific activity of GSTs (glutathione S-transferases) has been demonstrated (Munteanu et al., 2010). Those authors suggested that MRC-5 cells could counteract the oxidative stress induced by silica nanoparticles, as all other enzymatic activity is induced such as catalase and GPx (glutathione peroxidase). In view of all results, the oxidative stress plays only an important role in cell mortality induced by 20 nm nanoparticles, notably in LLC-PK_1. This is certainly due to the poor response of antioxidant systems with a single induction of catalase. A recent study with proteomic analysis showed that nano-SiO_2 (15 nm; 30 nm) exposure, which exerted toxic effects, altered the protein regulation of antioxidant protein such as thioredoxin reductase (Yang et al., 2010). This alteration was negatively correlated with SiO_2 particle size (15 nm >30 nm > micro-sized SiO_2). The antioxidant capacity in HK-2 was weakly solicited, leading to cytotoxicity of 20 nm nano-SiO_2 via disequilibrium in which reactive oxygen species generation overwhelmed the cellular antioxidant defense. This oxidative stress induced may lead to alteration in mitochondrial function as described in astrocytoma cells (Lai et al., 2010). The nano-SiO_2 exposure reduced expression of two essential proteins implicated in mitochondrial respiratory chain: cytochrome C oxidase II and NAPD dehydrogenase. Moreover, mitochondrial-involved apoptosis was observed with Bax induction, Bcl-2 inhibition and cytochrome c release in size-dependent manner (20 nm > 80 nm) (Lu et al., 2011).

The capacity of nano-SiO_2 internalization in kidney cells could lead to a large intracellular amount of nanoparticles, which would then give rise to huge ROS production. Therefore, a better understanding of the intracellular fate of nanoparticles, mainly determined by their endocytic pathway, is of great importance for investigating their toxic profile. To assess this question, we first verified whether fluorescent latex beads can be internalized in both cell types. The results demonstrated that particles internalization is possible in these cells. Previously, we showed that small particles (30 nm) are internalized in the cell cytoplasm (L'Azou et al., 2008). To identify the specific role of the endocytosis pathways involved in the cellular internalization of 100 nm nano-SiO_2, cells were treated with known biochemical inhibitors of its different pathways. Endocytosis pathways can be classified into macropinocytosis, clathrin- and caveolae-mediated endocytosis and cholesterol-rich microdomains. Macropinocytosis is an actin-dependent process that is not a specific transport system with formation of large heterogeneous dynamic vesicular structures at the cell surface, whose sizes ranges from 0.5 to 2 μm (Johannes and Lamaze, 2002). In that study, cytochalasin D, an inhibitor of actin polymerization classically reported to inhibit macropinocytosis and phagocytosis, induced a strong decrease of 100 nm nano-SiO_2 uptake. Pre-treatment of HaCaT cells (human keratinocyte cells) with cytochalasin D led to a dose-dependent inhibition of ROS generation normally obtained after exposure to 70 nm silica nanoparticles (Nabeshi et al., 2011). Recently, both the clathrin- and caveolae-mediated pathways have been shown to require actin for formation and invagination of both coated pits and caveosomes (Kaksonen et al., 2006). Then, inhibition of particle internalization by cytochalasin D may reflect inhibition of either macropinocytosis, clathrin-mediated or caveolae-mediated pathways, or a combination of the three. Indeed, the clathrin pathway is highly involved with a much-reduced uptake of nano-SiO_2 in the presence of chlorpromazin. Surprisingly, no significant inhibition of internalization in the presence of dynasore was observed. This could be due to the fact that as dynasore is a rapidly acting molecule, the incubation time used in this study (4 h) might have been too long to use such a molecule (Macia et al., 2006). Concerning another internalization pathway, endocytosis was improved with inhibitors based on cholesterol sequestration (providing a disorganization in caveolin molecules), suggesting a stimulation of an alternative endocytosis pathway or a disorder in the cell membrane integrity equilibrium. However, genistein induced a decrease in nanoparticle uptake but only in LLC-PK_1 cells. This apparent difference in the impact of genistein could be due to cell-type differences. A relevant issue with respect to the observation that caveolae are only present in specific cell types (Johannes and Lamaze, 2002). Thus, caveolae-dependent endocytosis would not seem to be highly involved in nano-SiO_2 internalization, which is coherent with data concerning the estimated size of caveolae-coated pits, ranging from 50 to 80 nm (Nichols, 2003; Lajoie and Nabi, 2007).

In conclusion, 20 nm silica nanoparticles possess notable cytotoxic effects whereas 100 nm ones appear less toxic. Furthermore, this toxicity is associated to stress oxidative with up-production ROS and lipid peroxidation. The low toxicity of 100 nm nano-SiO_2 could be due to induction of cellular detoxication process (thioredoxin reductase, GSTpi, catalase). By identifying the mechanisms of internalization, we show that silica nanoparticles predominantly penetrate the cells by maropinocytosis and clathrin-dependent endocytosis, resulting to intracellular localization into endocytosis vesicles as observed by Transmission Electron Microscope. Our findings also provide insights into tubular toxicity, an issue that has received little attention. Further studies are now needed to assess the impact of nanoparticles on glomerular section of the kidney.

Funding

This work was supported by MEEDDM (French Ministry: Ministère de l'Ecologie, de l'Energie, du Développement durable et de la Mer) in the INERIS program 189 "Nanotrans".

Competing interest

The authors declare that they have no competing interests.

Acknowledgements

We gratefully acknowledge Aurélien Auger for nano-SiO_2 synthesis. We thank the Hydrologie Environnement Laboratory (LHE) of the University of Bordeaux (UFR Pharmacy) for their help in turbidimetry experiments. Technical help for transmission and field electronic microscopy studies on nano-SiO_2 was provided by Elisabeth Sellier (CREMEM, France). We thank Bordeaux Imaging Center

for TEM cell observations. The authors thank JP. Lasserre for helpful English comments.

References

Akhtar, M.J., Ahamed, M., Kumar, S., Siddiqui, H., Patil, G., Ashquin, M., Ahmad, I., 2010. Nanotoxicity of pure silica mediated through oxidant generation rather than glutathione depletion in human lung epithelial cells. Toxicology 276, 95–102.

Antognelli, C., Gambelunghe, A., Del Buono, C., Murgia, N., Talesa, V.N., Muzi, G., 2009. Crystalline silica Min-U-Sil 5 induces oxidative stress in human bronchial epithelial cells BEAS-2B by reducing the efficiency of antiglycation and antioxidant enzymatic defenses. Chem. Biol. Interact. 182, 13–21.

Arslan, Z., Ates, M., McDuffy, W., Agachan, M.S., Farah, I.O., Yu, W.W., Bednar, A.J., 2011. Probing metabolic stability of CdSe nanoparticles: alkaline extraction of free cadmium from liver and kidney samples of rats exposed to CdSe nanoparticles. J. Hazard. Mater. 192, 192–199.

Auffan, M., Rose, J., Bottero, J.Y., Lowry, G.V., Jolivet, J.P., Wiesner, M.R., 2009a. Towards a definition of inorganic nanoparticles from an environmental, health and safety perspective. Nat. Nanotechnol. 4, 634–641.

Auffan, M., Rose, J., Wiesner, M.R., Bottero, J.Y., 2009b. Chemical stability of metallic nanoparticles: a parameter controlling their potential cellular toxicity in vitro. Environ. Pollut. 157, 1127–1133.

Auger, A., Samuel, J., Poncelet, O., Raccurt, O., 2011. A comparative study of non-covalent encapsulation methods for organic dyes into silica nanoparticles. Nanoscale Res. Lett. 6, 328.

Bradford, M.M., 1976. A rapid and sensitive method for the quantitation of microgram quantities of protein utilizing the principle of protein-dye binding. Anal. Biochem. 72, 248–254.

Castranova, V., 2004. Signaling pathways controlling the production of inflammatory mediators in response to crystalline silica exposure: role of reactive oxygen/nitrogen species. Free Radic. Biol. Med. 37, 916–925.

Chen, J., Dong, X., Zhao, J., Tang, G., 2009. In vivo acute toxicity of titanium dioxide nanoparticles to mice after intraperitoneal injection. J. Appl. Toxicol. 29, 330–337.

Chen, J.F., Ding, H.M., Wang, J.X., Shao, L., 2004. Preparation and characterization of porous hollow silica nanoparticles for drug delivery application. Biomaterials 25, 723–727.

Chen, Z., Meng, H., Xing, G., Chen, C., Zhao, Y., Jia, G., Wang, T., Yuan, H., Ye, C., Zhao, F., Chai, Z., Zhu, C., Fang, X., Ma, B., Wan, L., 2006. Acute toxicological effects of copper nanoparticles in vivo. Toxicol. Lett. 163, 109–120.

Cho, M., Cho, W.S., Choi, M., Kim, S.J., Han, B.S., Kim, S.H., Kim, H.O., Sheen, Y.Y., Jeong, J., 2009. The impact of size on tissue distribution and elimination by single intravenous injection of silica nanoparticles. Toxicol. Lett. 189, 177–183.

Cocco, P., 2001. Multifactorial aetiology of lung cancer among silica-exposed workers. Ann. Acad. Med. Singapore 30, 468–474.

Cocco, P., Dosemeci, M., Rice, C., 2007. Lung cancer among silica-exposed workers: the quest for truth between chance and necessity. Med Lav 98, 3–17.

dos Santos, T., Varela, J., Lynch, I., Salvati, A., Dawson, K.A., 2011. Effects of transport inhibitors on the cellular uptake of carboxylated polystyrene nanoparticles in different cell lines. PLoS One 6, e24438.

Eom, H.J., Choi, J., 2009. Oxidative stress of silica nanoparticles in human bronchial epithelial cell, Beas-2B. Toxicol. In Vitro 23, 1326–1332.

Fruijtier-Polloth, C., 2012. The toxicological mode of action and the safety of synthetic amorphous silica—a nanostructured material. Toxicology 294, 61–79.

Fuller, J.E., Zugates, G.T., Ferreira, L.S., Ow, H.S., Nguyen, N.N., Wiesner, U.B., Langer, R.S., 2008. Intracellular delivery of core-shell fluorescent silica nanoparticles. Biomaterials 29, 1526–1532.

Gong, C., Tao, G., Yang, L., Liu, J., He, H., Zhuang, Z., 2012. The role of reactive oxygen species in silicon dioxide nanoparticle-induced cytotoxicity and DNA damage in HaCaT cells. Mol. Biol. Rep. 39, 4915–4925.

Gonzalez, L., Thomassen, L.C., Plas, G., Rabolli, V., Napierska, D., Decordier, I., Roelants, M., Hoet, P.H., Kirschhock, C.E., Martens, J.A., Lison, D., Kirsch-Volders, M., 2010. Exploring the aneugenic and clastogenic potential in the nanosize range: A549 human lung carcinoma cells and amorphous monodisperse silica nanoparticles as models. Nanotoxicology 4, 382–395.

Gratton, S.E., Napier, M.E., Ropp, P.A., Tian, S., DeSimone, J.M., 2008. Microfabricated particles for engineered drug therapies: elucidation into the mechanisms of cellular internalization of PRINT particles. Pharm. Res. 25, 2845–2852.

Gunness, P., Aleksa, K., Kosuge, K., Ito, S., Koren, G., 2010. Comparison of the novel HK-2 human renal proximal tubular cell line with the standard LLC-PK1 cell line in studying drug-induced nephrotoxicity. Can. J. Physiol. Pharmacol. 88, 448–455.

Hansen, S.F., Michelson, E.S., Kamper, A., Borling, P., Stuer-Lauridsen, F., Baun, A., 2008. Categorization framework to aid exposure assessment of nanomaterials in consumer products. Ecotoxicology 17, 438–447.

He, X., Nie, H., Wang, K., Tan, W., Wu, X., Zhang, P., 2008. In vivo study of biodistribution and urinary excretion of surface-modified silica nanoparticles. Anal. Chem. 80, 9597–9603.

IARC, 1997. IARC Working Group on the evaluation of carcinogenic risks to humans: silica, some silicates, coal dust and para-aramid fibrils. Lyon, 15–22 October 1996. IARC Monogr. Eval. Carcinog. Risks Hum. 68, 1–475.

Johannes, L., Lamaze, C., 2002. Clathrin-dependent or not: is it still the question? Traffic 3, 443–451.

Kaksonen, M., Toret, C.P., Drubin, D.G., 2006. Harnessing actin dynamics for clathrin-mediated endocytosis. Nat. Rev. Mol. Cell Biol. 7, 404–414.

L'Azou, B., Jorly, J., On, D., Sellier, E., Moisan, F., Fleury-Feith, J., Cambar, J., Brochard, P., Ohayon-Courtes, C., 2008. In vitro effects of nanoparticles on renal cells. Part. Fibre Toxicol. 5, 22.

Lai, J.C., Ananthakrishnan, G., Jandhyam, S., Dukhande, V.V., Bhushan, A., Gokhale, M., Daniels, C.K., Leung, S.W., 2010. Treatment of human astrocytoma U87 cells with silicon dioxide nanoparticles lowers their survival and alters their expression of mitochondrial and cell signaling proteins. Int. J. Nanomed. 5, 715–723.

Lajoie, P., Nabi, I.R., 2007. Regulation of raft-dependent endocytosis. J. Cell. Mol. Med. 11, 644–653.

Lin, W., Huang, Y.W., Zhou, X.D., Ma, Y., 2006. In vitro toxicity of silica nanoparticles in human lung cancer cells. Toxicol. Appl. Pharmacol. 217, 252–259.

Lison, D., Thomassen, L.C., Rabolli, V., Gonzalez, L., Napierska, D., Seo, J.W., Kirsch-Volders, M., Hoet, P., Kirschhock, C.E., Martens, J.A., 2008. Nominal and effective dosimetry of silica nanoparticles in cytotoxicity assays. Toxicol. Sci. 104, 155–162.

Lu, X., Qian, J., Zhou, H., Gan, Q., Tang, W., Lu, J., Yuan, Y., Liu, C., 2011. In vitro cytotoxicity and induction of apoptosis by silica nanoparticles in human HepG2 hepatoma cells. Int. J. Nanomed. 6, 1889–1901.

Macia, E., Ehrlich, M., Massol, R., Boucrot, E., Brunner, C., Kirchhausen, T., 2006. Dynasore, a cell-permeable inhibitor of dynamin. Dev. Cell 10, 839–850.

Mamdouh, Z., Giocondi, M.C., Laprade, R., Le Grimellec, C., 1996. Temperature dependence of endocytosis in renal epithelial cells in culture. Biochim. Biophys. Acta 1282, 171–173.

Marano, F., Hussain, S., Rodrigues-Lima, F., Baeza-Squiban, A., Boland, S., 2010. Nanoparticles: molecular targets and cell signalling. Arch. Toxicol.

Moller, P., Jacobsen, N.R., Folkmann, J.K., Danielsen, P.H., Mikkelsen, L., Hemmingsen, J.G., Vesterdal, L.K., Forchhammer, L., Wallin, H., Loft, S., 2010. Role of oxidative damage in toxicity of particulates. Free Radic. Res. 44, 1–46.

Muller, D., Houpert, P., Cambar, J., Henge-Napoli, M.H., 2006. Role of the sodium-dependent phosphate co-transporters and of the phosphate complexes of uranyl in the cytotoxicity of uranium in LLC-PK1 cells. Toxicol. Appl. Pharmacol. 214, 166–177.

Munteanu, M., Radu, M., Hermenean, A., Sima, C., Dinu, D., Costache, M., Grigoriu, C., Dinischiotu, A., 2010. Antioxidative response induced by SiO_2 nanoparticles in MRC5 cell line. Romanian Biotechnol. Lett. 15, 5000–5007.

Nabeshi, H., Yoshikawa, T., Matsuyama, K., Nakazato, Y., Arimori, A., Isobe, M., Tochigi, S., Kondoh, S., Hirai, T., Akase, T., Yamashita, T., Yamashita, K., Yoshida, T., Nagano, K., Abe, Y., Yoshioka, Y., Kamada, H., Imazawa, T., Itoh, N., Tsunoda, S., Tsutsumi, Y., 2010. Size-dependent cytotoxic effects of amorphous silica nanoparticles on Langerhans cells. Pharmazie 65, 199–201.

Nabeshi, H., Yoshikawa, T., Matsuyama, K., Nakazato, Y., Tochigi, S., Kondoh, S., Hirai, T., Akase, T., Nagano, K., Abe, Y., Yoshioka, Y., Kamada, H., Itoh, N., Tsunoda, S., Tsutsumi, Y., 2011. Amorphous nanosilica induce endocytosis-dependent ROS generation and DNA damage in human keratinocytes. Part. Fibre Toxicol. 8, 1.

Napierska, D., Thomassen, L.C., Lison, D., Martens, J.A., Hoet, P.H., 2010. The nanosilica hazard: another variable entity. Part. Fibre Toxicol. 7, 39.

Nichols, B., 2003. Caveosomes and endocytosis of lipid rafts. J. Cell Sci. 116, 4707–4714.

Nishimori, H., Kondoh, M., Isoda, K., Tsunoda, S., Tsutsumi, Y., Yagi, K., 2009. Silica nanoparticles as hepatotoxicants. Eur. J. Pharm. Biopharm. 72, 496–501.

Park, Y.H., Kim, J.N., Jeong, S.H., Choi, J.E., Lee, S.H., Choi, B.H., Lee, J.P., Sohn, K.H., Park, K.L., Kim, M.K., Son, S.W., 2010. Assessment of dermal toxicity of nanosilica using cultured keratinocytes, a human skin equivalent model and an in vivo model. Toxicology 267, 178–181.

Passagne, I., Evrard, A., Winum, J.Y., Depeille, P., Cuq, P., Montero, J.L., Cupissol, D., Vian, L., 2003. Cytotoxicity, DNA damage, and apoptosis induced by new fotemustine analogs on human melanoma cells in relation to O_6-methylguanine DNA-methyltransferase expression. J. Pharmacol. Exp. Ther. 307, 816–823.

Powers, K.W., Brown, S.C., Krishna, V.B., Wasdo, S.C., Moudgil, B.M., Roberts, S.M., 2006. Research strategies for safety evaluation of nanomaterials. Part VI. Characterization of nanoscale particles for toxicological evaluation. Toxicol. Sci. 90, 296–303.

Pujalte, I., Passagne, I., Brouillaud, B., Treguer, M., Durand, E., Ohayon-Courtes, C., L'Azou, B., 2011. Cytotoxicity and oxidative stress induced by different metallic nanoparticles on human kidney cells. Part. Fibre Toxicol. 8, 10.

Rabolli, V., Thomassen, L.C., Princen, C., Napierska, D., Gonzalez, L., Kirsch-Volders, M., Hoet, P.H., Huaux, F., Kirschhock, C.E., Martens, J.A., Lison, D., 2010. Influence of size, surface area and microporosity on the in vitro cytotoxic activity of amorphous silica nanoparticles in different cell types. Nanotoxicology 4, 307–318.

Rabolli, V., Thomassen, L.C., Uwambayinema, F., Martens, J.A., Lison, D., 2011. The cytotoxic activity of amorphous silica nanoparticles is mainly influenced by surface area and not by aggregation. Toxicol. Lett. 206, 197–203.

Rejman, J., Oberle, V., Zuhorn, I.S., Hoekstra, D., 2004. Size-dependent internalization of particles via the pathways of clathrin- and caveolae-mediated endocytosis. Biochem. J. 377, 159–169.

Roger, E., Lagarce, F., Garcion, E., Benoit, J.P., 2009. Lipid nanocarriers improve paclitaxel transport throughout human intestinal epithelial cells by using vesicle-mediated transcytosis. J. Control. Release 140, 174–181.

Ryan, M.J., Johnson, G., Kirk, J., Fuerstenberg, S.M., Zager, R.A., Torok-Storb, B., 1994. HK-2: an immortalized proximal tubule epithelial cell line from normal adult human kidney. Kidney Int. 45, 48–57.

Shang, Y., Zhu, T., Li, T., Zhao, J., 2009. Size-dependent hydroxyl radicals generation induced by SiO_2 ultra-fine particles: the role of surface iron. Sci. China Ser. B: Chem. 52, 1033–1041.

Steenland, K., Rosenman, K., Socie, E., Valiante, D., 2002. Silicosis and end-stage renal disease. Scand. J. Work. Environ. Health 28, 439–442.

Ushio-Fukai, M., 2006. Localizing NADPH oxidase-derived ROS. Sci. STKE 2006, re8.
Vercauteren, D., Piest, M., Al Soraj, M., Jones, A.T., Engbersen, J.F., De Smedt, S.C., Braeckmans, K., 2010. Unraveling the cellular uptake of bioreducible poly(amido amine)–gene complexes in cells of the retinal pigment epithelium. J. Control. Release 148, e99–e100.
Wang, F., Gao, F., Lan, M., Yuan, H., Huang, Y., Liu, J., 2009a. Oxidative stress contributes to silica nanoparticle-induced cytotoxicity in human embryonic kidney cells. Toxicol. In Vitro 23, 808–815.
Wang, F., Jiao, C., Liu, J., Yuan, H., Lan, M., Gao, F., 2009b. Oxidative mechanisms contribute to nanosize silican dioxide-induced developmental neurotoxicity in PC12 cells. Toxicol. In Vitro 23, 808–815.
Wang, J., Zhou, G., Chen, C., Yu, H., Wang, T., Ma, Y., Jia, G., Gao, Y., Li, B., Sun, J., Li, Y., Jiao, F., Zhao, Y., Chai, Z., 2007. Acute toxicity and biodistribution of different sized titanium dioxide particles in mice after oral administration. Toxicol. Lett. 168, 176–185.
Waters, K.M., Masiello, L.M., Zangar, R.C., Tarasevich, B.J., Karin, N.J., Quesenberry, R.D., Bandyopadhyay, S., Teeguarden, J.G., Pounds, J.G., Thrall, B.D., 2009. Macrophage responses to silica nanoparticles are highly conserved across particle sizes. Toxicol. Sci. 107, 553–569.
Yang, X., Liu, J., He, H., Zhou, L., Gong, C., Wang, X., Yang, L., Yuan, J., Huang, H., He, L., Zhang, B., Zhuang, Z., 2010. SiO_2 nanoparticles induce cytotoxicity and protein expression alteration in HaCaT cells. Part. Fibre Toxicol. 7, 1.
Ye, Y., Liu, J., Xu, J., Sun, L., Chen, M., Lan, M., 2010. Nano-SiO_2 induces apoptosis via activation of p53 and Bax mediated by oxidative stress in human hepatic cell line. Toxicol. In Vitro 24, 751–758.